Proceedings of ASME Turbo Expo 2011
GT2011
June 6-10, 2011, Vancouver, British Columbia, Canada

GT2011-45284

COMPUTATIONAL STUDY OF KELVIN-HELMHOLTZ INSTABILITY CREATED BY INTERACTION OF THE MAINSTREAM FLOW AND THE SEAL FLOW IN GAS TURBINES

M. Rabs, F.-K. Benra, C. Domnick
Email: michael.rabs@uni-due.de
Chair of Turbomachinery
University of Duisburg-Essen
47048 Duisburg, Germany

O. Schneider
Email: oliverschneider@siemens.com
Siemens AG, Power Generation
Gas Turbine Technology
45473 Mülheim, Germany

ABSTRACT

The present paper gives a contribution to a better understanding of the emergence of Kelvin-Helmholtz instabilities (KHI) in gas turbines. In an earlier paper of the authors, the occurrence of the KHI´s near the rim cavity of a 1.5 stage gas turbine has been examined by use of CFD methods. It is shown that the KHI´s occur, when the swirl component of the hot gas flow is very strong. Due to the fact, that a high swirl is produced by the guide vanes of the first stage, this matter concerns all common gas turbines.

In order to get a basic theoretical background of the emergence of the KHI´s, 2D CFD investigations of the flow behind a splitter plate have been performed showing the development of KHI´s downstream of the splitter plate. To validate the numerical results a comparison to test rig data is used. This shows that the numerical method can simulate the characteristics of the KHI´s. Furthermore, a parameter study is conducted to extract parameters describing the appearance of KHI's, the vortex periodicity and stability criteria.

The main intention of this paper is to deliver "KHI parameters", which are able to describe the development of the KHI in gas turbine rim cavities.

KEYWORDS

Gas Turbine, Hot Gas Ingestion, Kelvin-Helmholtz Instability

INTRODUCTION

The improvement of the aerodynamic performance of gas turbine rim seals is subject of many technical papers. A better understanding of the flow through the rim seals leads to a better reliability of the design and therefore serves for higher machine performance.

One important matter is the prevention of hot gas ingestion through the rim seals. The ingestion through the seal clearance is a complex process and has to be avoided at any time of turbine operation. The flow between vanes and blades at the rim of the main annulus comprises complex time-dependent and three-dimensional pressure and velocity fields. To understand the flow development and the interaction between the cavity flow and the main annulus a lot of turbine well studies were conducted in the past. Most of the studies dealt with experimental and numerical investigations of hot gas ingestion into the rim cavity. Physical models and correlations have been developed to estimate the amount of required coolant flow to gain acceptable temperatures of the rotor and stator walls of the cavity. Owen and Rogers [1], [2] provide many experimental data and give a fundamental analysis of the flow and heat transfer in rotor-stator cavities. Furthermore, there are a lot of studies, which investigated unsteady effects of rim cavity flow. Numerical studies of Jacobi et al. [3] and Cao et al. [4] observed large scale rotating structures in the cavity, which increases the hot gas ingestion, due to the low pressure region in the center of those large scale structures. Nevertheless, the common knowledge of the underlying phenomena driving ingestion is still not complete and a better understanding of the complex flow physics is necessary, particularly regarded to unsteady flow phenomena. The actual study of the authors aims to contribute toward achieving this objective.

The present paper gives a contribution to the comprehension of the interaction of sealing air and the hot gas in the gap between rotor and stator. The interaction of the sealing air and the hot gas at the rim has an impact on the flow field at the rim and can produce coherent vortex structures. Rabs et al. [5] identified these coherent vortex structures as so called Kelvin-Helmholtz vortices. They showed that the KH vortices occur near the rim cavity, when the tangential component of the hot gas is very strong and a minimum mass flow rate of sealing air exists. The requirement for the development of KHI is the existence of a shear layer, which is a result of two parallel, superposed flows with different velocities. A strong swirl is produced by the guide vanes of the first stage of nearly all common gas turbines. The nearly tangential hot gas flow together with the nearly tangential seal air flow (due to the rotor turning) produces a superposed shear flow in the gap area, so that KHI´s are developing and coherent vortex structures occur. An example for the development of the KHI´s in a real engine environment is depicted in Fig. 1. It shows a contour plot of the static pressure in a plane in the direction of the hot gas flow in an engine CFD model. The establishment of the KHI´s can be clearly seen in the gap area and in the hot gas path.

The KHI´s can influence the hot gas ingestion, as the vortices are developing in the gap region. Fig. 2 shows the pressure distribution in an engine rim seal environment with simplified boundary conditions. The underlying model neglects the vanes and blades and uses as hot gas boundary conditions surface averaged parameters. Here the propagation of the vortices can be clearly seen along the circumference. Due to the emergence of the vortices in the gap, the cavity is sealed by the vortices along the complete circumference. Including the three dimensional, unsteady effect of the vanes and the blades the vortices do not propagate along the complete circumference, just locally and temporally. Nevertheless, there would be parts along the circumference, where the cavity is sealed by the KH vortices.

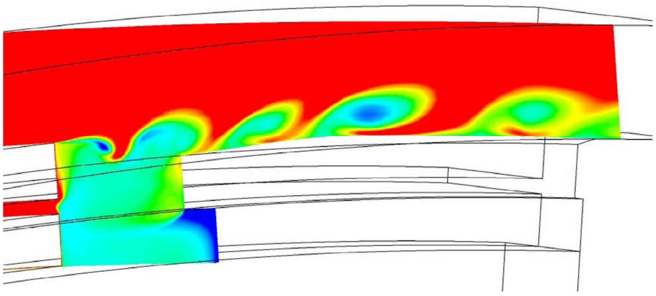

Fig. 1: Contour Plot static pressure in the gap and the hot gas path of a real engine [6]

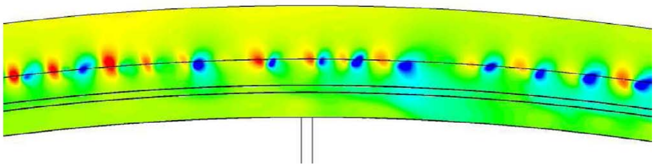

Fig. 2: Contour plot of static pressure in an r-φ plane in the gap region and hot gas path [6]

Fig. 3: Kelvin-Helmholtz clouds
Photo: National center for atmospheric research, USA

The phenomenon of KHI is not limited to gas turbine rim cavities. Such vortex structures occur in the nature as well. For example, they can be observed in the atmosphere, where the characteristic clouds formation appears (Fig. 3). Furthermore, they can be observed in technical applications, e.g. on separation bubbles, on airfoils or in liquid-gas interfaces in process engineering systems. Due to the general significance of this topic many experimental and theoretical studies have been performed in the past. For example, Turner [7] and Lugt [8] provide fundamental, theoretical background of the formation of KHI´s. Some experimental studies are dealing with the investigation of KHI´s on a laminar separation bubble [9], in the flow field over a delta wing [10] and on the flow field behind a splitter plate [11].

Unfortunately there were no experimental, theoretical or numerical investigations about the emergence of KHI´s in gas turbine rim cavities conducted in the past. To the knowledge of the authors, for the first time a contribution for a better understanding of the development of KHI´s in gas turbine rim cavities is given in the present paper. The first step is to find out which parameters and methods can picture the development of the KHI´s with satisfiying quality. Due to the absence of experimental studies of KHI´s in gas turbine rim cavities, the experiments conducted by Bonnet et al. [11] have been chosen to validate the numerical methods used for the investigations in this paper. Bonnet et al. [11] investigated experimentally the emergence of the vortices in the resulting shear layer behind a splitter plate. In this paper, a parameter study is conducted to point out sensitive parameters for the appearance, periodicity and stability of the vortices. The parameter study is performed using splitter plate models, which have their basis in the model used for the test rig validation. The investigation on a splitter plate model has the advantage, that the extraction of interesting KHI parameter (e.g. frequency, vortex velocity) can be performed comparatively easily. The next step will be the extraction of KHI parameters of a gas turbine rim cavity model, which will include a comparison with KHI parameters of the splitter plate model discussed below. This is an actual study of the authors but not part of the present paper.

NOMENCLATURE

Arabic and Greek letters

c	Vortex velocity	m/s
f	Frequency	Hz
r	Velocity ratio	-

r	Radius	m
u, v	Velocity	m/s
x, y, z	Coordinate	m
y+	Non- dimensional wall distance	-
A	Discretization step size	-
E_u	Frequency spectra of u	Hz
E_v	Frequency spectra of v	Hz
T	Temperature	K
δ_ω	Vorticity thickness	mm
λ	Vortex distance	m
ρ	Density	kg/m^3
σ	Measurement uncertainty	-
φ	Angle	°
Δu	Velocity difference	m/s

Subscripts

1, a	Upper splitter passage
2, b	Lower splitter passage
m	medial

Abbreviations

2D	2-Dimensional
CFD	Computational Fluid Dynamics
CEAT	Aeronautical testing center
Det.	Determinant of elements
KHI	Kelvin-Helmholtz instability
PFD	Pseudo Flow Visualitzation
RMS	Root mean square

TEST RIG VALIDATION

Data used to evaluate the model described herein are obtained at the C.E.A.T.- Laboratoire d´Etudes Aérodynamiques. The test rig is described by Bonnet et al. [11]. A cross section of the test rig, employed for the experiments, is shown in Fig. 5 for reference. Coherent vortex structures have been examined, which are developing between two streams with velocities of U_a=42.2 m s^{-1} and U_b=25.2 m s^{-1}. In the apparatus, the streams are separated at the beginning using a splitter plate. At the trailing edge of the plate the streams are merging to a free shear layer with a velocity ratio $r=U_a/U_b$=0.59. In this area the vortex development has been investigated. The stream velocities have been measured using multi-probe hot wires. Specially designed rakes of hot-wires have been built at the C.E.A.T. by Delville et al. [12]. The hot wires (W-Pt) have a length of 0.5 mm and a diameter of 2.5 µm. T.S.I. 1750 anemometers with band-widths greater than 50 kHz are used. Measurements of the unsteady velocity components u and v have been performed. The frequency spectra of these components were investigated using a Fourier analysis. It was pointed out that the frequency of the vortices corresponds with the dominant frequency of the velocity components.

Numerical approach

2D-time-dependent numerical simulations of the flow field are performed with the Ansys CFX12.0 release code. This code uses a segregated, fully coupled Navier-Stokes solver with implicit linearization. The turbulence is modeled by a standard k-ε turbulence model. The spatial discretization scheme is of second order accuracy and the second order backward Euler scheme was used for the time-dependent calculation. The convergence criteria for the time-dependent simulation are a maximum RMS value smaller than 10^{-3} in each time step for all flow residuals. A sensitive study concerning the choice of the time step shows that a time step of $5{\cdot}10^{-5}$ s is of convenient amount. The operating point is first calculated using a steady state model to get appropriate initial values for the time-dependent calculation. The solution convergence for the steady state calculation is monitored by the history of the flow residuals and is obtained when the flow residuals fall below the value of 10^{-4} of the maximum RMS residuals. The convergence for the time-dependent calculation is reached after approximately 2000 time steps, when a time periodic flow field is obtained.

Subject of the simulation is the red framed part in Fig. 5, which is called “square test section”. Fig. 6 shows the geometry and the boundary conditions of the numerical model. Additional boundary conditions are given in Table A 1. Furthermore, the positions of the measuring points are depicted, which are taken for the analysis of the unsteady data. The fluid is air, treated as ideal gas with constant material properties (perfect gas). The temperature is 300 K for both streams. Concerning the investigation of KHI the effects of friction at the outer boundaries of the numerical model, Wall Top and Wall Bottom, can be neglected. This provokes a coarser resolution of the grid next to the outer walls and consequently lowers the computational effort. The grid is generated using Ansys Icem12.0 release code. It is block structured and exclusively hexahedral elements are used. From a grid sensitive study the most appropriate grid considering low computational effort and high quality results is identified to have a total node number of 458,200. The maximum y+ value is 1.6 and the minimum orthogonality angle is 86 degree. . The grid resolution around the splitter plate is shown in Fig. 4. Further grid properties can be found in Table A 2.

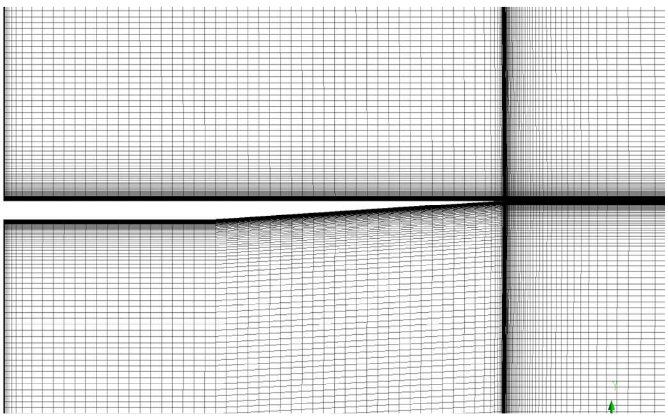

Fig. 4: Grid resolution around splitter plate

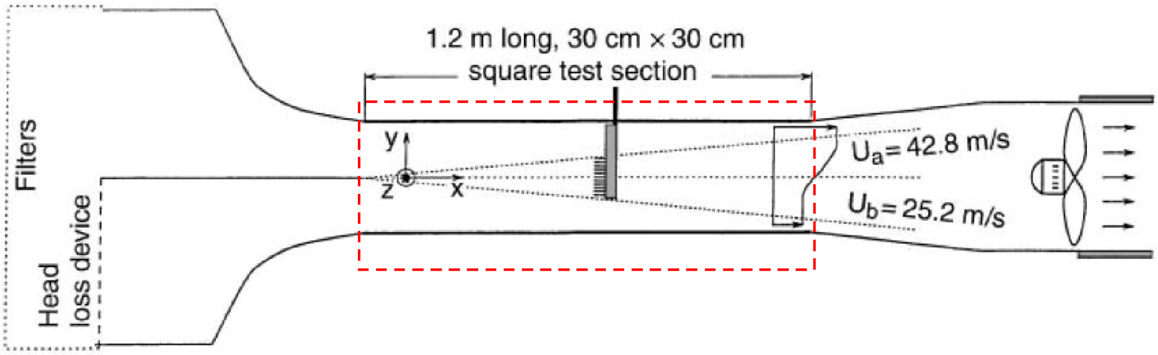

Fig. 5: Experimental configuration [11]

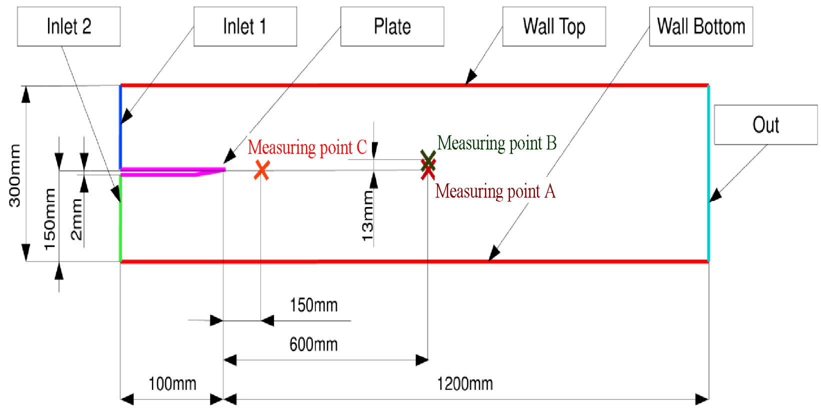

Fig. 6: Geometry and boundary conditions of numerical model (not to scale)

Comparison between experiment and CFD simulation

To validate the numerical results, a comparison with experimental data from the test rig at the C.E.A.T.- Laboratoire d´Etudes Aérodynamiques is conducted. The frequency spectrum is determined using a discrete Fourier transformation. Furthermore, the vorticity thickness is calculated and a comparison using the Pseudo Flow Visualization (PFD) takes place.

Four frequency spectra are extracted from the experiments for the velocity components u und v. The underlying measuring parameter and positions are listed in Table A 3. The origin is the trailing edge of the plate and the coordinate system is defined according to Fig. 5. The y-coordinate is transformed dimensionless using the vorticity thickness δω, which is defined in equ. (1).

For the comparison the corresponding velocity components are read out from the CFX-Solver. 2048 time steps are considered. This results in a spectral resolution of 9.8 Hz for the Fourier transformation. The comparison of the experimental and the numerical results is depicted in Fig. 7. The colored lines illustrate the numerical results of the spectral analysis and the black lines with symbols display the experimental ones. Both the abscissa and the ordinate have a logarithmic scale. The simulation results of component $E_u(f)y/\delta_\omega$~0 match the experimental results relatively well, but for the range smaller than 200 Hz the difference is relatively high. The simulation results of component $E_v(f)y/\delta_\omega$~0 of the measured frequency spectrum are also inaccurate. Especially the peak at 478 Hz is to be mentioned. The peak is in the same range of the maximum value as for the measured frequency spectrum, but for the numerical results no dominant frequency is observed. Furthermore, there are significant discrepancies for the frequency range between 10 Hz and 200 Hz. But overall, a sufficient coincidence is obtained. For the frequency spectra, extracted from the outer area of the shear layer (Measuring point B), it is also obvious that the dominant frequency is not so strong deflected by the measured results compared to the simulation results. Furthermore, the first harmonic (at 900 Hz) is not observed by the experiments. But overall, the frequency spectrum lines of the simulations follow the principal characteristics of the measured frequency spectra.

An explanation of the deviation between the measured frequency spectra and the simulated frequency spectra could be the sensitivity of the discrete Fourier transformation. Furthermore, the numbers of time steps in the experiments are much higher than the time steps calculated in the simulation. The time record lengths of the data are 819200 time steps (more than 80 s) for the low sampling frequency (10 kHz) and 10240 time steps (about 0.1 s) for the high sampling frequency (100 kHz). To obtain this data quantity, a simulation would run approximately 14 month by use of 8 computer cores of today´s development level. Furthermore, band pass filter are used to filter interferences. For this reason the simulation results are less proper evaluated compared to the measured results. Presumably, the simulation describes the dominant frequency more exact, because it does not consider all real occurring processes as e.g. effects from the three dimensional behavior of the real flow. These and other effects, which are present in the experiment, could be the reason that there is no strong peak in the experiments.

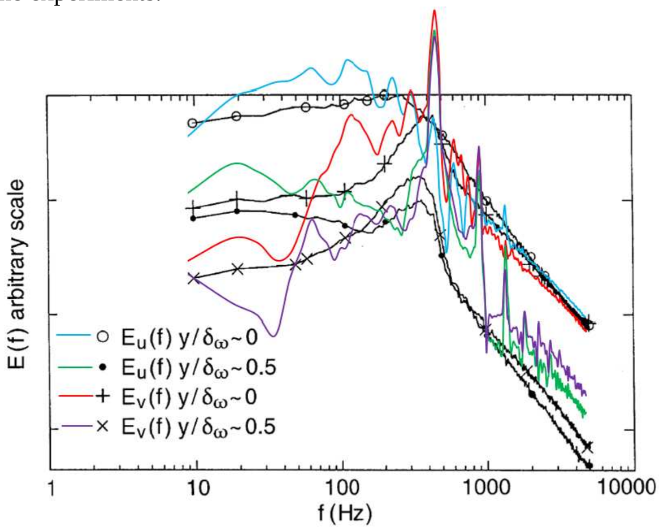

Fig. 7: Fourier analysis of velocity components u and v, on the axis (y/δ_w=0) and on the middle of the mixing layer (y/δ_w=0.5) for experiment and CFD simulation

In addition to the frequency spectra, the vorticity thickness is determined. The vorticity thickness δω is defined as the quotient of the velocity difference Δu and the partial derivation of the velocity component u in the middle of the shear layer with respect to y (equ. (1)). The stronger the development of the vortices, the higher is the vorticity thickness.

$$\delta_\omega = \frac{\Delta u}{\left.\frac{\partial u}{\partial y}\right|_{y=0}} \tag{1}$$

Due to the time-averaged nature of the vorticity thickness, a steady state simulation is used for the evaluation. Fig. 8 depicts the downstream evolution of the vorticity thickness. It can be seen that the simulation results match the experimental results very good.

The use of dense rakes of probes combined with high speed simultaneous sampling is a way to determine accurately the space-time evolution of the flow field [13], at least for the large scale organization of the flow. Bonnet et al. [11] used the "Pseudo Flow Visualization" (PFV) technique to picture velocity vectors. For details of the technique see [11]. For the experiment, the velocities are measured in the shear layer 600 mm downstream of the trailing edge of the splitter plate using 24 hot-wire anemometers. Twelve anemometers are used for the evaluation of the velocity component u and twelve are used for the velocity component v. From the unsteady measurement data, velocity vector plots are generated by use of the PFV.

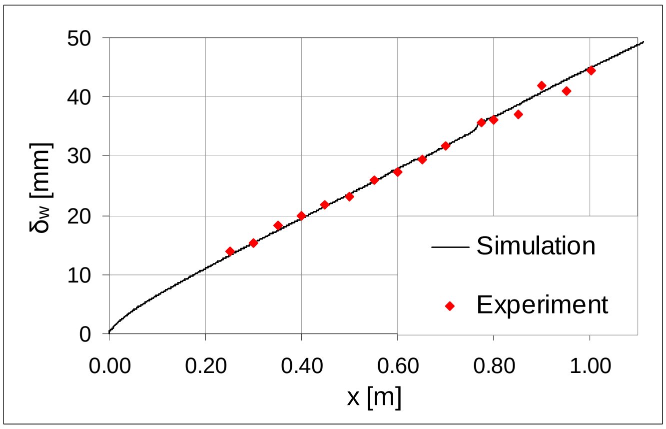

Fig. 8: Downstream evolution of vorticity thickness δ_w for experiment and CFD simulation

For a better comparison, the vector plot of the simulation is generated using the PFV technique as well. Fig. 9 shows the experimental result and the simulation result. It is noticeable that the measured PFV illustration is very chaotic in comparison to the simulated illustration. But the simulation pictures in average the vortex magnitude and the vortex distances relatively good.

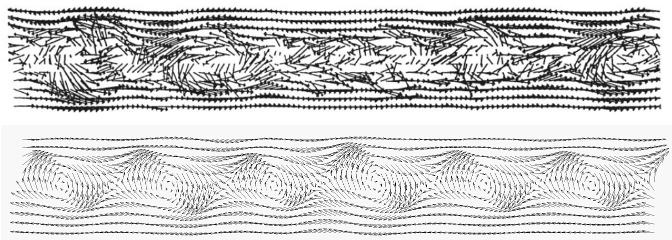

Fig. 9: Comparison of Pseudo Flow Visualization for experiment (top) and CFD simulation (down)

PARAMETER STUDY

The parameter study contains a variation of the velocity and the temperature of streams u_1 and u_2 and a variation of the pressure. All models used for the parameter studies are based on the numerical model of the test rig validation.

For the analysis the vortex distance λ, the dominant vortex frequency f at measuring point A and the vortex velocity $c=\lambda \cdot f$ are examined. The measurement uncertainty of the vortex velocity is calculated with equ. (2) using the law of error propagation. The relative error of the determination of the vortex distances is assumed as ±1%. For the discrete Fourier transformation the error is considered as the discretization error, which is half of the step size A. All measuring uncertainties are pictured in all diagrams as black bars.

$$\sigma(c) = \lambda \frac{A}{2} + 0.01 \cdot \lambda \cdot f \tag{2}$$

Velocity variation

Basically, two different simulation sets are conducted. For the first one u_1 is kept constant with 20 m/s and u_2 is varied. For the second one u_1 is kept constant with 50 m/s and u_2 is varied again. An overview of the performed simulations with the appropriate velocity pairs is shown in Table 1. Furthermore, a third simulation set is performed. The aim of this investigation is to check if there is any minimum difference velocity, where KHI may occur. Therefore, u_1 is set to 50 m/s and u_2 is decreased from 55 m/s in the beginning to 52 m/s, 51 m/s and 50 m/s finally. The temperature is 300 K for both streams and the outlet pressure is 1 bar for all simulation sets.

u_1 [m/s]	u_2 [m/s]	u_m [m/s]	r
20	30	25	1.5
20	40	30	2
20	50	35	2.5
20	60	40	3
50	75	62.5	1.5
50	100	75	2
50	125	87.5	2.5
50	150	100	3
50	50-55	50-52.5	1-1.1

Table 1: Velocity configurations

Fig. 10 shows the vortex distance versus the average velocity. It can be seen that there is a linear relation between the vortex distance and the average velocity u_m. The vortex distance increases with increasing average velocities. The formula for the regression line is defined by equ. (4). The vortex frequency behaves a somewhat different (see Fig. 9). For velocity pairs which average amount is higher than u_m= 62.5 m/s a linear relation can be observed. In this range of high u_m the rule is: the higher u_m the lower is the frequency. But this rule does not match for the frequencies which exist for small u_m. Here, no relation between vortex frequency and average velocity can be derived. As an overall result it is to mention that the frequency seems to decrease with increasing average velocity.

Fig. 12 shows the vortex velocity versus the average velocity of both streams. Here it can be pointed out that the vortex velocity equates the average velocity ($c=u_m$). This is also a result of the inviscid Kelvin-Helmholtz shear layer theory. Turner (7) derived a correlation for the vortex velocity, which is defined in equ. (3). Calculating the vortex velocity with this equation by use of the density and the velocity of the CFD results, the vortex velocity matches the simulation vortex velocity c==λ·f quite well (not presented). Equ. (3) shows that the vortex velocity is affected by the single velocities and single densities of each streams.

$$c = u_m = \frac{\rho_1 u_1 + \rho_2 u_2}{\rho_1 + \rho_2} \qquad (3)$$

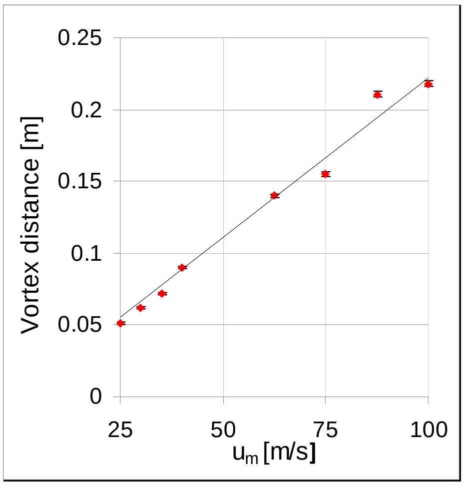

Fig. 10: Vortex distance vs. average velocity with regression line

$$\lambda = 0.002182 \cdot u_m \qquad (4)$$

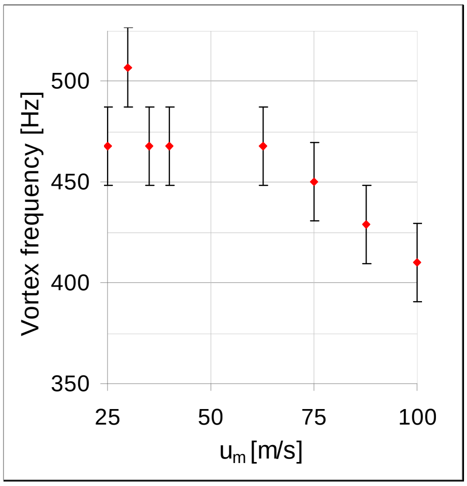

Fig. 11: Vortex frequency vs. average velocity

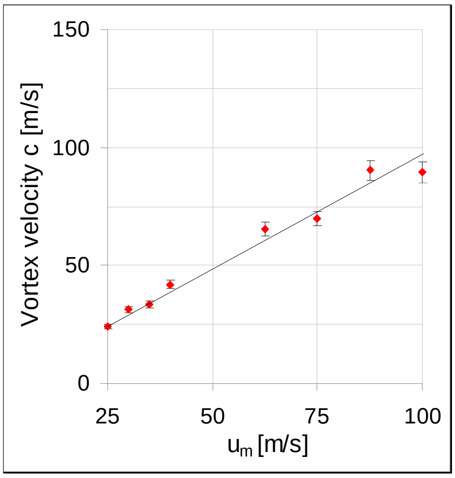

Fig. 12: Vortex velocity vs. average velocity with regression line

The investigation concerning the minimum velocity difference shows that vortices also occur at equal velocities for both streams. This is an interesting result, since two different velocities are essential for a development of KHI´s. But the vortex pattern is a somehow different compared to the KHI´s. This can be seen in Fig. 13. Here, the vortices change their rotational direction which leads to alternating vortices, while a KHI develops with one rotational direction for all vortices. This vortex structure seems to arise from the trailing vortices. Due to the boundary layer of the splitter plate, vorticity is produced in the flow on both sides of the splitter plate. The interaction of both vorticity fields (positive and negative) produces trailing vortices after merging behind the trailing edge of the splitter plate. Theoretical background concerning trailing vortices can be found in [8]. The trailing vortices are developed for the velocity pair 50/51 m/s. The velocity pair 50/52 m/s is dominated by the KH vortices, but first signs of trailing vortices can be noticed.

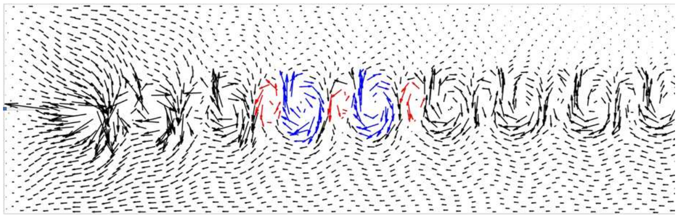

Fig. 13: Velocity vectors for equal flow velocities

Pressure variation

For this investigation, simulations with three different outlet pressure values are presented. Starting with 1 bar, the pressure is increased to 10 bar and 20 bar. The temperature of the air is kept constant with 300 K for both streams and the stream velocities are u_1=50 m/s and u_2=75 m/s.

For the analysis the velocity component v is read out along the x-axis. Fig. 14 shows the downstream evolution of the velocity component v for different pressures. It can be seen that the pressure level does not impact the behavior of the velocity profile and consequently does not impact the development of the KHI´s. In addition, the frequency spectra of the velocity component v are depicted in Fig. 15. In contrast to Fig. 14 there are small differences between the curves due to the sensitivity of the discrete Fourier transformation. The independence of the KHI concerning the pressure shown here is consistent with the common theory, that not the absolute density of the flow is important, but the density difference of both streams influences the development of KHI.

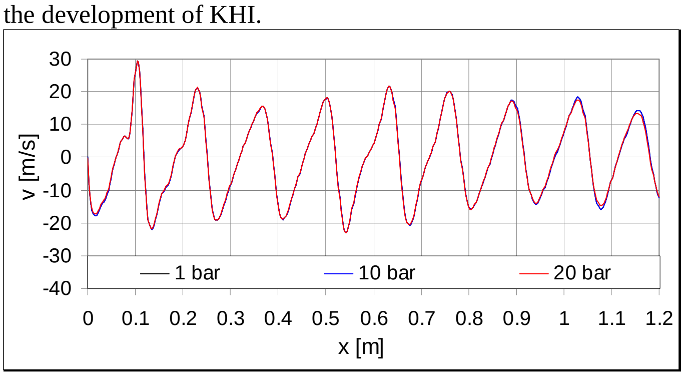

Fig. 14: Downstream evolution of v for different pressures

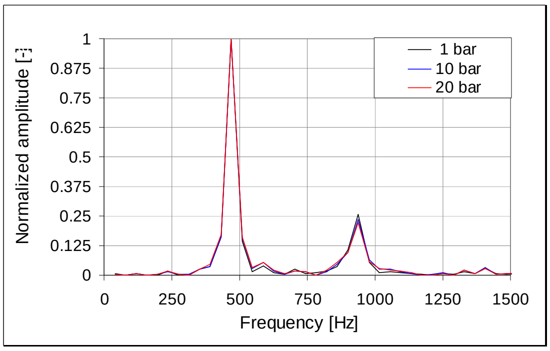

Fig. 15: Frequency spectra of velocity component v for different pressures

Uniform temperature variation

For this investigation the temperatures of both streams are increased equally. Four different temperatures have been investigated (300 K, 900 K, 1200 K and 1500 K). The stream velocities are u_1=50 m/s and u_2=75 m/s and the outlet pressure is 1 bar.

Fig. 16 shows the vortex distance versus the temperature. It is obvious that the vortex distance decreases with increasing temperature. Equ. (5) defines the formula for the regression line and gives a linear relation between the vortex distance and the temperature.

The vortex frequencies increase with increasing temperature, which can be seen in Fig. 17. Here, the vortex frequency is plotted versus the temperature. Equ. (6) gives a linear relation between the vortex frequency and the temperature.

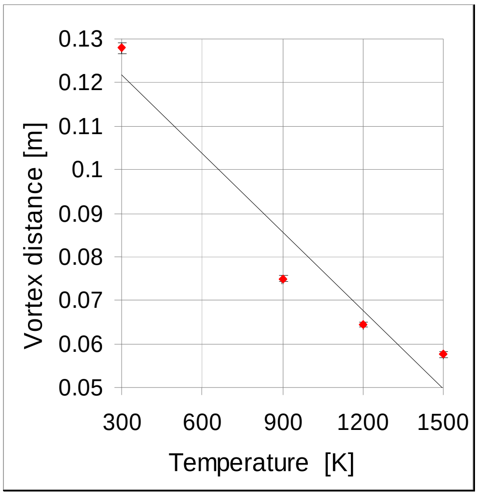

Fig. 16: Vortex distance vs. temperature with regression line

$$\lambda = -6 \cdot 10^{-5} \cdot T + 0.1398 \qquad (5)$$

The vortex velocity c for all cases averages 60.07 m/s. This value is very close to the average velocity of 62.5 m/s. The standard deviation of the models of this evaluation is 1.46 m/s. For this reason it is obvious that standard deviation is in the range of the calculation uncertainty. According to that, the vortex velocity is constant, and consequently no function of the temperature. The vortex velocity versus the temperature is depicted in Fig. 18.

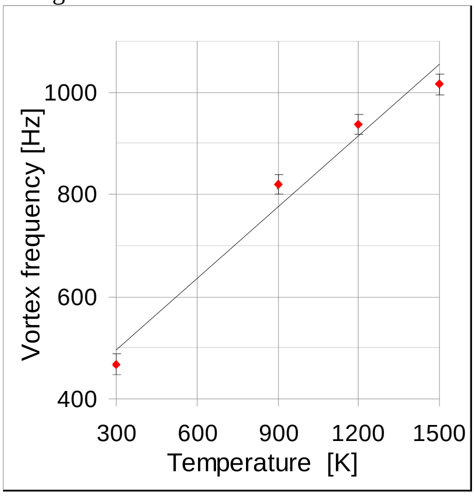

Fig. 17: Vortex frequency vs. temperature with regression line

$$f = 0.4561 \cdot T + 356.1 \qquad (6)$$

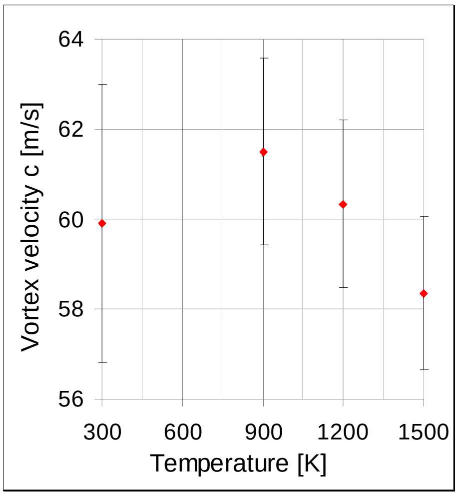

Fig. 18: Vortex velocity vs. temperature

Non-uniform temperature variation

For this investigation the temperatures of both streams are varied differently. The following temperature pairs are examined: 300/300 K, 300/600 K, 300/900 K, 300/1200 K. Again the stream velocities are u_1=50 m/s and u_2=75 m/s and the outlet pressure is 1 bar.

Fig. 19 shows that the vortex distance decreases with decreasing average temperatures. The resulting linear correlation is given by equ. (7). Surprisingly, the regression formula of equ. (5) and equ. (7) are nearly identical. Consequently, it can be assumed that the influence of the temperature to the vortex distance can be well quantified.

The vortex frequencies increase with increasing temperatures, which can be taken from Fig. 20. Here, the vortex frequency is shown versus the temperature. Equ. (8) gives a linear relation between the vortex frequency and the temperature. Due to the high similarity, the regression line of equ. (6) is added in Fig. 20 in red color.

The vortex velocity again is not a function of the average temperature. The vortex velocities are in the range of the average velocity of 62.5 m/s. The error bars can be seen in Fig. 21.

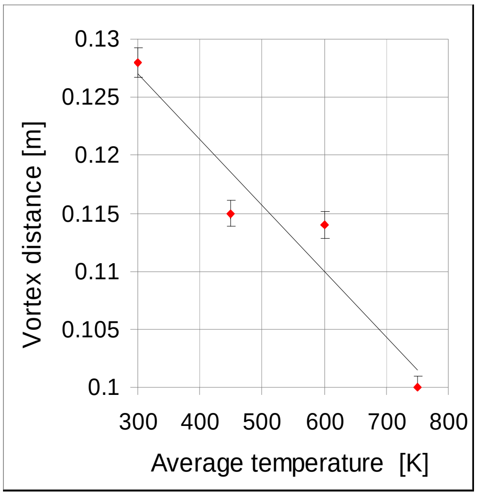

Fig. 19: Vortex distance vs. average temperature with regression line

$$\lambda = -6 \cdot 10^{-5} \cdot T_m + 0.144 \qquad (7)$$

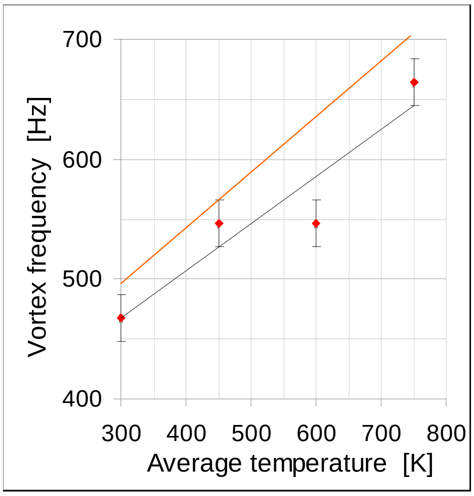

Fig. 20: Vortex frequency vs. average temperature with regression lines (red: Uniform temperature variation; black: Non-uniform temperature variation)

$$f = 0.329 \cdot T_m + 350.2 \qquad (8)$$

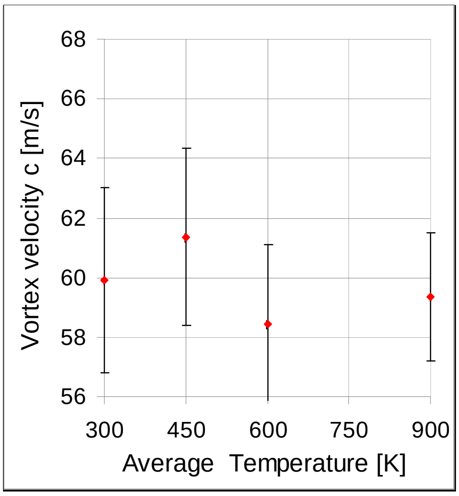

Fig. 21: Vortex velocity vs. average temperature

CONCLUSIONS AND OUTLOOK

The development of KHI´s behind a splitter plate is investigated and characterized using numerical methods. A test rig validation shows that the applied numerical methods can picture the important characteristics of KHI´s. A parameter study, for which the velocity, the temperature and the pressure are varied, provides linear functions for the vortex distance, the vortex frequency and the vortex velocity in dependency of the average velocity, respectively the average temperature.

The next step of the authors is the extraction of KHI parameters for a gas turbine rim cavity model. Here, a comparison with the KHI parameters of the splitter model will be carried out. The KHI´s seem to have a strong influence on the flow in the gap region of the rim cavity. Due to the fact that only the guide vanes produce an extreme swirl, only front cavities (rim cavity between guide vane and blade) are influenced by this matter. Due to the occurrence of the KHI´s in the seal gap along the circumference, those can prevent the deep ingestion of hot gas into the cavity. Furthermore, the KHI´s also influence the flow of the hot gas path. Due to the downstream development of the vortices, they cross the blades passages and decrease the efficiency of this blade passage. One further important matter is the noise stress, which arise from the KHI´s. Sukhinin et al. [14] showed that coherent vortex structures in shear layers are responsible for the emergence of noise. In order to develop low noise engines, it is important to understand the emergence of those structures and if necessary to avoid them.

All this effects could have an impact on the future development of gas turbine engines. For this reason it is required to get a fundamental background of the KHI development and behavior in gas turbine rim cavities as well. This makes it necessary to continue the investigation of KHI´s in gas turbine rim cavities.

REFERENCES

1. Owen, J.M.; Rogers, R.H. (1989), *Flow and heat transfer in rotating-disc systems, Volume 1-rotor-stator systems,* Research studies press; Taunton, Somerset (UK)
2. Owen, J.M.; Rogers, R.H. (1995), *Flow and heat transfer in rotating-disc systems, Volume 2-rotating cavities,* Research studies press; Taunton, Somerset (UK)
3. Jacoby, R., Zierer, T., Lindblad, K., Larsson, J., deVito, L., Bohn, D.E., Funcke, J. and Decker, A. (2004), *Numerical simulation of the unsteady flow field in an axial gas turbine rim seal configuration,* Proceedings of 2004 ASME Turbo Expo, GT2004-53829
4. Cao, C., Chew, J.W., Millington, P.R., Hogg, S.I. (2004), *Interaction of rim seal and annulus flow in an axial flow turbine,* J. of Eng. for Gas Turbines and Power, vol 109 (1098), August, pp. 786-793
5. Rabs, M.; Benra, F.-K.; Dohmen, H.J.; Schneider, O. (2009), *Investigation of flow instabilities near the rim cavity of a 1.5 stage gas turbine*, Proceedings of 2009 ASME Turbo Expo, GT2009-59965
6. Rabs, M. (2008), Numerische Untersuchung der Strömung in durch Rotorscheiben gebildete Kavitäten von Gasturbinen im Hinblick auf Heißgaseinzug [Numerical investigation of hot gas ingress of gas turbine rim cavities], Diploma Thesis, University of Duisburg-Essen
7. Turner, J.S. (1973), *Buoyancy effects in fluids: Instability and the production of turbulence*, Cambridge University press
8. Lugt, J. (1979), *Wirbelströmung in Natur und Technik [Vortex flow in nature and engineering]*, Braun
9. Marxen, O.; Lang. M.; Rist, U.; Wagner, S. (2003), *A combined experimental/Numerical study of unsteady phenomena in a laminar separation bubble,* Flow, Turbulence and Combustion, vol 71, pp. 133-146

10 Riley, A.J..; Lowson. M.V. (1998), *Development of a three-dimensional free shear layer*, Journal of Fluid Mechanics, vol 369, pp. 49-89

11 Bonnet, J.P.; Delville, J.; Garem, J.H. (1998), *Collaborative testing of eddy structure identification methods in free turbulent shear flows,* Experiments in Fluids, vol.25, pp. 197-225

12 Delville, J.; Bellin, S.; Bonnet, J.P. (1989), *Analysis of structures in a turbulent, plane mixing layer by use of pseudo visualization method based on hot-wire anemometry,* Advances in turbulence, vol.2, pp. 251-256

13 Glauser, M.N.; George, W.K. (1992), *Application of multipoint measurements for flow characterization,* Experimental Thermal Fluid Sci, vol. 5, pp. 617-632

14 Sukhinin, S.V.; Bardakhanov, S.P. (1998), *Aeolian tones of a plate in a channel*, Journal of Applied Mechanics and Technical Physics, vol. 39, Bd.2, pp. 220-227

ANNEX A

Name	Type	Parameter	
Inlet 1	Inlet	Flow regime	Subsonic
		Velocity	42.8 m/s
		Temperature	300K
		Turbulence	Medium (5%)
Inlet 2	Inlet	Flow regime	Subsonic
		Velocity	25.2 m/s
		Temperature	300K
		Turbulence	Medium (5%)
Plate	Wall	Friction	No slip
		Roughness	Smooth
		Heat conduction	Adiabat
Wall Top	Wall	Friction	Free slip
		Roughness	Smooth
		Heat conduction	Adiabat
Wall Bottom	Wall	Friction	Free slip
		Roughness	Smooth
		Heat conduction	Adiabat
Out	Outlet	Flow regime	Subsonic
		Static pressure	1 bar

Table A 1: Boundary conditions of splitter plate model

Mesh	Nodes	max. y+	Nodes x	Nodes y	Angle	Aspect ratio	Quality	Det	Vol.change
B	458,200	1.6	609	400	86.87	248	0.99	0.99	3.0

Table A 2: Grid parameter

Description according to [11]	Velocity component	x-coordinate	Dimensionless y-coordinate	y-coordinate	Measuring point
$E_u(f)y/\delta_\omega$~0	u	600 mm	0	0 mm	A
$E_u(f)y/\delta_\omega$~0.5	u	600 mm	0.5	13 mm	B
$E_v(f)y/\delta_\omega$~0	v	600 mm	0	0 mm	A
$E_v(f)y/\delta_\omega$~0.5	v	600 mm	0.5	13 mm	B

Table A 3: Coordinates of measuring points